

# Equilibrium fluid-solid coexistence of hard spheres

L. A. Fernandez,<sup>1,2</sup> V. Martin-Mayor,<sup>1,2</sup> B. Seoane,<sup>1,2</sup> and P. Verrocchio<sup>3,4,5,2</sup>

<sup>1</sup>*Departamento de Física Teórica I, Universidad Complutense, 28040 Madrid, Spain.*

<sup>2</sup>*Instituto de Biocomputación y Física de Sistemas Complejos (BIFI), Spain.*

<sup>3</sup>*Dipartimento di Fisica, Università di Trento, via Sommarive 14, I-38050 Povo, Trento, Italy.*

<sup>4</sup>*Istituto Sistemi Complessi (ISC-CRS), UOS Sapienza, Via dei Taurini 19, 00185 Roma, Italy.*

<sup>5</sup>*Interdisciplinary Laboratory for Computational Physics (LISC), Trento, Italy.*

We present a tethered Monte Carlo simulation of the crystallization of hard spheres. Our method boosts the traditional umbrella sampling to the point of making practical the study of constrained Gibbs' free energies depending on several crystalline order-parameters. We obtain high-accuracy estimates of the fluid-crystal coexistence pressure for up to 2916 particles (enough to accommodate fluid-solid interfaces). We are able to extrapolate to infinite volume the coexistence pressure ( $p_{co} = 11.5727(10)k_B T/\sigma^3$ ) and the interfacial free energy ( $\gamma_{\{100\}} = 0.636(11)k_B T/\sigma^2$ ).

PACS numbers: 05.10.Ln, 64.60.-i, 64.60.My, 64.70.D-.

Crystallization is a vast field of research, where experiments and theory cross-fertilize. Hard-spheres (HS) provide a celebrated example: the numerical finding of a fluid-solid phase transition [1] motivated experiments on colloids [2, 3]. Finding an accurate procedure to locate the equilibrium phase boundaries for HS is a crucial step to address the self-assembly of complex molecules [4], as modeled by HS plus non-spherical interactions (e.g patchy [5] and Janus particles [6]).

Up to now, numerical simulations of crystallization phase transitions have been well behind their fluid-fluid counterpart (e.g. vapor-liquid equilibria [7]). Actually, HS are the preferred benchmark for numerical approaches to crystallization. Yet, the lack of exact solutions enhances the importance of accurate numerical and/or experimental studies.

However, for preexisting numerical methods, a simulation whose starting configuration is a fluid never reaches the equilibrium crystal. Much as in experiments [3], the simulation gets stuck in a metastable crystal, or a defective crystal (or even a glass [8]). The proliferation of metastable states defeats optimized Monte Carlo (MC) methods that overcome free-energy barriers in simpler systems [9–11]. Besides, experimental and numerical determinations of the interfacial free energy are plainly inconsistent (maybe due to a small electrical charge in the colloidal particles [12]).

Since feasible numerical methods [13] could not form the correct crystalline phase spontaneously, choosing the starting particle configuration became an issue (e.g. crystalline or a carefully crafted mixture of solid and fluid phases). Methods can be classified as *equilibrium* or *nonequilibrium*. In the phase switch MC [14], one tries to achieve fluid-crystal equilibrium (only up to  $N = 500$  HS [15]). An alternative is the separate computation of the fluid and solid free energies, supplemented with the conditions of equal pressure, temperature and chemical potential. For the fluid's free energy, one resorts to thermodynamic integration, while choices are available for the crystal (Wigner-Seitz [16], Einstein crystal [17, 18], Einstein molecule [19]). The nonequilibrium *direct coex-*

*istence* method [20, 21] handles larger systems [22].

As for the accuracy, in equilibrium computations the coexistence pressure  $p_{co}$  was obtained with precisions of  $\sim 0.1\%$  (at finite  $N$ ). Yet, the  $N$  values that can be simulated are rather small. An  $N \rightarrow \infty$  extrapolation is mandatory, which degrades the final accuracy to  $\sim 1\%$  [14, 15, 19] (results are summarized in Table I). The situation improves by an order of magnitude for the direct-coexistence method. With the exception of [15], the different estimations of  $p_{co}$  are compatible, although with widely differing accuracies.

The computation of the interfacial free energy,  $\gamma$ , is more involved, since the issue of spatially heterogeneous mixtures of fluid and solid can no longer be skipped (as done in equilibrium computations of  $p_{co}$ ). Indeed, recent estimations are either precise but mutually incompatible [23, 24], or of lesser accuracy [25].

Here, we introduce a tethered MC [26, 27] approach to HS crystallization. The correct crystal appears in our simulation by constraining the value of two order parameters. At variance with preexisting methods, the crystal found is independent from the starting particle configuration. Tethered MC provides a major simplification for the standard umbrella sampling method [28, 29]: chemical-potential differences among fluid and crystal are very precisely computed from a thermodynamic integration. In fact, our method resembles studies of liquid-vapor equilibria [30, 31]. We go continuously from the fluid to the crystal by varying a reaction coordinate that labels the intermediate states. Rather than particle density, our reaction coordinate is a blend of bond-orientational crystal order parameters with different symmetries [32–34]. Very accurate determinations of the coexistence pressure and the interfacial free energy follow. The number of HS ranges  $108 \leq N = 4n^3 \leq 4000$ , ( $n$  integer). Our largest systems do show the surface-driven geometric transitions characteristic of the asymptotic large  $N$  regime [35–37].

We consider  $N$  hard spheres of diameter  $\sigma$ , at constant pressure  $p$ , in a cubic box with periodic boundary conditions. The equilibrium crystal is face-centered cubic (FCC) [38]. With the shorthand  $\mathbf{R}$  for the particle

positions,  $\{\mathbf{r}_i\}_{i=1}^N$ , Gibbs free energy  $g(p, T)$  is given by

$$e^{-N\beta g(p, T)} = \frac{p\beta}{N!\Lambda^{3N}} \int_0^\infty dV e^{-\beta pV} \int d\mathbf{R} H(\mathbf{R}), \quad (1)$$

( $\Lambda$ : de Broglie thermal wavelength,  $\beta = 1/(k_B T)$  and  $H(\mathbf{R}) = 0$  if any pair of spheres overlaps, or 1 otherwise).

We loosely constraint the values of two global order parameters,  $Q_6$  and  $C$ . The well-known  $Q_6$  detects the spatially coherent alignment of nearest-neighbors bonds in a lattice [32, 33]. It is the  $l = 6$  instance of

$$Q_l \equiv \sqrt{\frac{4\pi}{2l+1} \sum_{m=-l}^l \left| \frac{\sum_{i=1}^N \sum_{j=1}^{N_b(i)} Y_l^m(\hat{r}_{ij})}{\sum_{i=1}^N N_b(i)} \right|^2}, \quad (2)$$

( $Y_l^m(\hat{r}_{ij})$ : spherical harmonics;  $\hat{r}_{ij}$ : unitary vector pointing from particle  $i$  to particle  $j$ ;  $N_b(i)$ : number of neighbors of particle  $i$  [39]).  $Q_6$  is positive in a crystal, while it is negligible ( $Q_6 \sim 1/\sqrt{N}$ ) in a fluid. Yet,  $Q_6$ 's rotational invariance is a nuisance: enforcing a large  $Q_6$  causes a crystal grain to grow in the fluid, but its orientation in the simulation box is arbitrary. In fact, when the grain finally hits itself through the periodic box's boundaries, long-lived metastable helicoidal crystals appear. The cure is an order parameter with only cubic symmetry [34]:

$$C = \frac{2288}{79} \frac{\sum_{i=1}^N \sum_{j=1}^{N_b(i)} c_\alpha(\hat{r}_{ij})}{\sum_{i=1}^N N_b(i)} - \frac{64}{79}, \quad (3)$$

where  $c_\alpha(\hat{r}) = x^4 y^4 (1 - z^4) + x^4 z^4 (1 - y^4) + y^4 z^4 (1 - x^4)$ .  $C = 1$  in an ideal, well aligned FCC, while  $C \approx 0$  for a fluid. Constraining a large  $C$  value suffices to obtain a nice crystal, irrespectively of the starting configuration (either a gas or an FCC structure). Still,  $Q_6$  helps us label unambiguously the intermediate states between the fluid and the FCC: some helicoidal crystals and the fluid-solid mixtures differ on their  $Q_6$  values (but not on  $C$ ).

To enforce the quasi-constraints  $C(\mathbf{R}) \approx \hat{C}$ ,  $Q_6(\mathbf{R}) \approx \hat{Q}_6$  [26, 27], first multiply the integrand in Eq. (1) by

$$1 = \frac{N\alpha}{2\pi} \int d\hat{Q}_6 d\hat{C} e^{-\frac{N\alpha}{2} [(\hat{Q}_6 - Q_6(\mathbf{R}))^2 + (\hat{C} - C(\mathbf{R}))^2]}. \quad (4)$$

The tunable parameter  $\alpha$  tightens the quasi-constraints (we choose  $\alpha = 200$  [27]). Exchanging the integration order in (1) yields

$$e^{-N\beta g(p, T)} = \int d\hat{Q}_6 d\hat{C} e^{-N\Omega_N(\hat{Q}_6, \hat{C}, p)}, \quad (5)$$

where the *effective potential*,  $\Omega_N(\hat{Q}_6, \hat{C}, p)$  is given by

$$e^{-N\Omega_N} = \frac{p\beta N\alpha}{2\pi N!\Lambda^{3N}} \int d\mathbf{R} dV \omega(\mathbf{R}, V; \hat{Q}_6, \hat{C}, p), \quad (6)$$

$\omega(\mathbf{R}, V; \hat{Q}_6, \hat{C}, p)$  being the *tethered weight* [40]

$$\omega = H(\mathbf{R}) e^{-\beta pV - \frac{N\alpha}{2} [(\hat{Q}_6 - Q_6(\mathbf{R}))^2 + (\hat{C} - C(\mathbf{R}))^2]}. \quad (7)$$

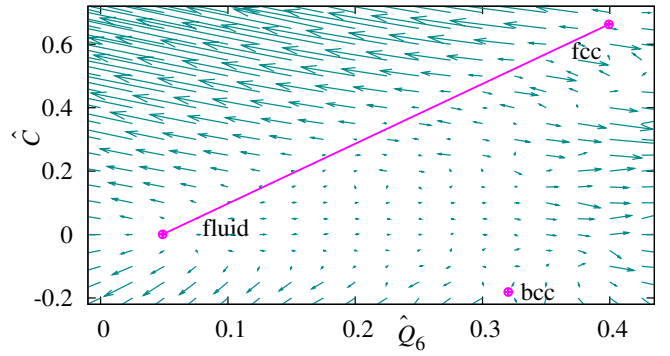


FIG. 1. (Color online) Vector field  $\nabla\Omega_N$  as computed from Eq. (8), for a system of  $N = 256$  hard-spheres, at the coexistence pressure for the fluid-FCC phase transition (we scaled  $\nabla\Omega_N$  with a factor  $1/\alpha$ ). Both the fluid and the FCC crystal are local minima of the effective potential, where  $\nabla\Omega_N = 0$ . The BCC coordinates are from  $N = 250$ .

Our method relies on Fluctuation-Dissipation formulae [26, 27], obtained by taking derivatives in Eq. (6). We compute the gradient of  $\Omega_N$  at fixed pressure from:

$$\nabla\Omega_N(\hat{Q}_6, \hat{C}) = \alpha(\langle \hat{Q}_6 - Q_6(\mathbf{R}) \rangle, \langle \hat{C} - C(\mathbf{R}) \rangle). \quad (8)$$

Coordinates  $(\hat{Q}_6^*, \hat{C}^*)$  of local minima of  $\Omega$  are located through  $\nabla\Omega_N = 0$ . Furthermore, differences  $\Omega_N(\hat{Q}_6^b, \hat{C}^b) - \Omega_N(\hat{Q}_6^a, \hat{C}^a)$  at fixed  $p$  are computed as the line integral of  $\nabla\Omega_N$  along any convenient path joining  $(\hat{Q}_6^a, \hat{C}^a)$  with  $(\hat{Q}_6^b, \hat{C}^b)$  in the  $(\hat{Q}_6, \hat{C})$  plane.

The chemical potential  $g(p, T)$  is obtained from a saddle-point expansion in Eq. (5). Up to corrections vanishing as  $1/N$ ,  $\beta g(p, T)$  is the absolute minimum of  $\Omega_N(p, \hat{Q}_6, \hat{C})$ . Yet, close to phase coexistence,  $\Omega_N$  has two relevant minima (i.e. the fluid and the FCC crystal). Therefore, the coexistence pressure  $p_{co}^{(N)}$  follows from  $\Omega_N^{\text{fluid}} = \Omega_N^{\text{FCC}}$  (i.e. equal chemical potential).

Our Metropolis MC simulation follows standard methods [7]. We recast  $\omega$  in Eq. (7) as the Boltzmann factor for HS at fixed pressure with a *fictive* potential energy  $k_B T N \alpha [(\hat{Q}_6 - Q_6(\mathbf{R}))^2 + (\hat{C} - C(\mathbf{R}))^2]/2$ . Since  $Q_6(\mathbf{R})$  and  $C(\mathbf{R})$  are built out of sums of local terms, the number of operations needed to compute their changes after a single-particle displacement does not grow with  $N$ .

Our framework is illustrated in Fig. 1, where we show  $\nabla\Omega_N(\hat{Q}_6, \hat{C})$  at  $p = p_{co}^{(N)}$ . We identify two local minima where  $\nabla\Omega_N = 0$  [the fluid, close to  $(\hat{Q}_6, \hat{C}) = (1/\sqrt{N}, 0)$ , and the FCC minimum where both parameters are positive]. Note their distance to other local minima of  $\Omega_N$ , such as the body centered cubic (BCC).

Our main goal is to compute  $\Delta\Omega(p) = \Omega^{\text{FCC}} - \Omega^{\text{fluid}}$ , choosing the straight segment in Fig. 1 as integration path. The path is parameterized by our *reaction coordinate*,  $S$  ( $S = 0$ : fluid,  $S = 1$ : FCC). Actually, due to the *additivity* of  $Q_6$  and  $C$ , choosing this segment is a must if we are to compute the interfacial free energy [41]. Indeed, physical fluid-solid coexistence is a convex combination of the two pure phases [42], which provides a

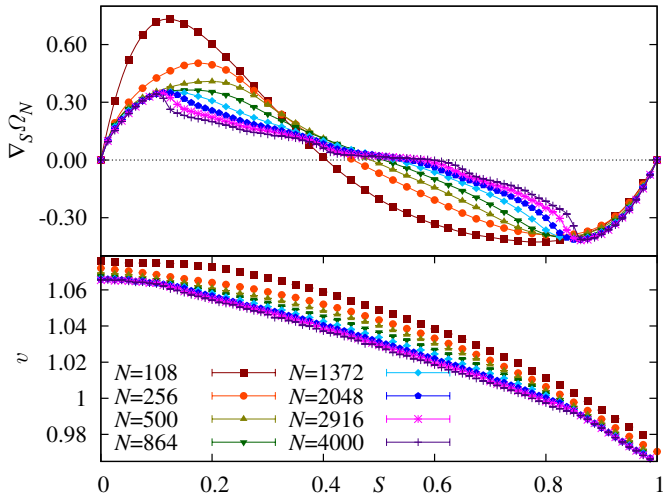


FIG. 2. (Color online) **(Top)**  $\nabla_S \Omega_N$  projected over the liquid-FCC line,  $\nabla_S \Omega_N$ , vs. the line parameter  $S$  ( $S = 0$ : fluid,  $S = 1$ : FCC), for all our system sizes at the simulation pressures. **(Bottom)** Specific volume  $v = V/N$  as a function of line parameter  $S$ . At large  $N$ ,  $v$  becomes a linear function, as expected for a convex combination of pure phases [42].

physical interpretation for  $S$  as the fraction of particles in the coexisting solid phase: in the large  $N$  limit,  $v$ ,  $C$  and  $Q_6$  vary linearly with  $S$  (see Fig. 2—bottom).

Our simulation set up is as follows. We start by locating  $(\hat{Q}_6, \hat{C})$  for the FCC and liquid minima at  $p \approx p_{co}^{(N)}$ . The first guess is obtained from  $NpT$  simulations with crystalline/disordered starting configurations. We later refine by solving for  $\nabla_S \Omega_N = 0$  [27].

Next, we introduce a uniform  $S$  grid on the liquid-FCC line and perform *independent* simulations at fixed  $(\hat{Q}_6, \hat{C}, p)$  (see Appendix A for simulation details). As a test for equilibration, achieved for all  $N$  but  $N = 4000$ , every run was performed twice (starting from an ideal gas or from an ideal FCC crystal) [43].

Now, at variance with umbrella sampling,  $\Delta\Omega(p)$  follows from the integral over  $0 \leq S \leq 1$  of  $\nabla_S \Omega_N$ , the projection of  $\nabla \Omega_N$  along the straight-line, Fig. 2—top. We use *reweighting* extrapolations [27, 44] to obtain  $\Delta\Omega(p)$  as a function of pressure. Then, it is easy to locate  $p_{co}^{(N)}$ , Fig. 3. Statistical errors are estimated as in [11].

We obtain  $p_{co} = 11.5727(10)$  in units of  $k_B T / \sigma^2$ , in the large- $N$  limit. This result is six times more accurate than the best nonequilibrium estimate,  $p_{co} = 11.576(6)$  [22] and improves by a factor of 90 over the equilibrium estimate,  $p_{co} = 11.49(9)$  [14]. We compute  $p_{co}$  through a fair fit ( $\chi^2 = 2.61$  for three degrees of freedom) of the  $p_{co}^{(N)}$  listed in Table I to a second order polynomial in  $1/N$  [45].

As for the interfacial free energy,  $\gamma$ , we need to consider inhomogeneous configurations [46]. In fact, due to the periodic boundary conditions, at intermediate  $S$  the surface energy is minimized by mixed configurations where a crystalline slab (or cylinder, or bubble) is surrounded by fluid, see the snapshots in Appendix B. As in vapor-liquid equilibria [31, 37], transitions among different ge-

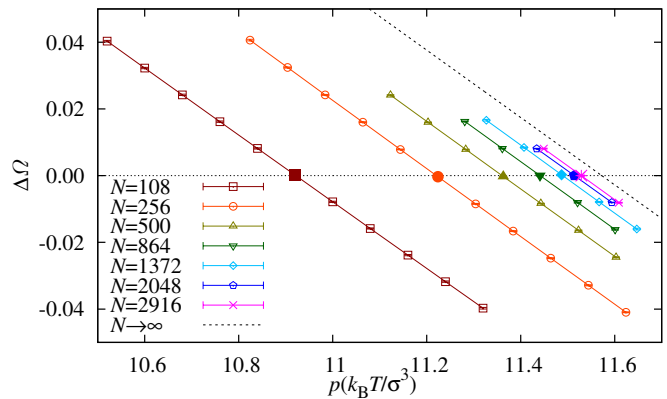


FIG. 3. (Color online) Effective-potential difference  $\Delta\Omega(p) = \Omega^{\text{FCC}} - \Omega^{\text{fluid}}$ , as a function of pressure. At  $p_{co}^{(N)}$ ,  $\Delta\Omega_N = 0$ . The large  $N$  limit stems from  $\Delta\Omega(p) = (v^{\text{FCC}} - v^{\text{fluid}})(p - p_{co}) / (k_B T) + \mathcal{O}((p - p_{co})^2)$ . The simulated pressures (see Table I) correspond to the larger, filled symbols.

ometries arise when  $S$  is varied. These transitions result in the cusps and steps that appear for large  $N$  in  $\nabla_S \Omega_N$ , Fig. 2—top, and can be detected as well through the fluctuations of the particle density [27]. Under these circumstances,  $\gamma$  may be computed using Binder’s method [47]. The effective potential has a local maximum along the line that joins the FCC and the fluid (the solution of  $\nabla_S \Omega_N = 0$  at  $S^* \approx 0.5$ , Fig. 2—top). The excess free energy is due to the *two* interfaces that the fluid presents with a crystalline slab parallel to the simulation box ( $\{100\}$  planes). Then the interfacial free energy at  $p_{co}^{(N)}$  is

$$\gamma^{(N)} = k_B T N (\Omega_{s^*} - \Omega_{\text{FCC}}) / (2 \langle N v \rangle_{S^*}^{2/3}). \quad (9)$$

The  $\gamma^{(N)}$  (listed in Table I) are extrapolated as [48]

$$\frac{\gamma^{(N)} \sigma^2}{k_B T} = \frac{\gamma \sigma^2}{k_B T} + \frac{a_2 - \log N}{6N^{2/3}} + \frac{a_3}{N} + \frac{a_4}{N^{4/3}} + \dots \quad (10)$$

A fit for  $256 \leq N \leq 2916$  yields  $\gamma = 0.636(11)$  in units of  $k_B T / \sigma^2$  ( $\chi^2 = 0.14$  for two degrees of freedom). We remark that the difference among the fit and  $\gamma^{(N=4000)}$  is one fifth of the error bar (Table I). Also, the extrapolation for  $500 \leq N \leq 2916$  merely doubles the final error estimate. Our result is compatible with  $\gamma = 0.64(2)$  [25] and  $\gamma = 0.619(3)$  [24], but not with  $\gamma = 0.5820(19)$  [23]. We remark that the  $\gamma^{(N)}$  estimation is fairly sensitive to  $p$  [27], an effect not systematically considered in [23–25]. Note that Eq. (10) holds if  $\gamma^{(N)}$  is computed at  $p_{co}^{(N)}$ .

A final warning is in order. Not much is known about the effect of the  $\nabla_S \Omega_N$ ’s cusps and steps, Fig. 2—top, in the large- $N$  extrapolation  $\gamma^{(N)} \rightarrow \gamma$ . This non-smoothness is a consequence of the geometric transitions that arise in our larger systems. However, the analogy with simpler models [11] (e.g. the  $D = 2$  Potts model, where comparison with exact solutions is possible), strongly suggests that these cusps and steps are inconsequential for the  $p_{co}^{(N)} \rightarrow p_{co}$  extrapolation.

$N$	$p^{\text{simulation}}$	This work				[14]	[15]	[22]	[19]
		$\langle v \rangle^{\text{FCC}}$	$\langle v \rangle^{\text{fluid}}$	$\gamma_{\{100\}}$	$p_{\text{co}}$	Phase switch		Direct coexistence	E. M.
108	10.92	0.97580(7)	1.07611(8)	0.4063(12)	10.9216(18)	10.94(4)	11.00(6)		11.02(5)
256	11.224	0.97049(6)	1.07202(7)	0.4243(8)	11.2209(13)	11.23(4)	11.25(1)		11.26(5)
500	11.363	0.96796(10)	1.06932(7)	0.4798(8)	11.3607(8)		11.34(1)		11.35(3)
864	11.441	0.96796(10)	1.06932(7)	0.5285(12)	11.4416(13)				
1372	11.487	0.96549(14)	1.06659(13)	0.5611(14)	11.4897(13)				11.50(3)
2048	11.514	0.96500(14)	1.06577(15)	0.5832(10)	11.5146(7)				11.52(3)
2916	11.529	0.96468(14)	1.06545(19)	0.5971(12)	11.5311(15)				
4000	11.54	0.96461(13)	1.06556(15)	0.607(2)	11.5452(11)				
$\infty$		0.96405(3)	1.06448(10)	0.636(11)	11.5727(10)	11.49(9)	11.43(2)	11.576(6)	11.54(4)
$\chi^2/\text{degrees of freedom}$		0.32/3	0.61/2	0.14/2	2.61/3				

TABLE I. For each  $N$ , we report the simulated pressure in units of  $k_B T / \sigma^3$ , the specific volume of the coexisting phases, the  $\{100\}$  surface tension  $\gamma_{\{100\}}$  (in  $k_B T / \sigma^2$  units) and the phase-coexistence pressure  $p_{\text{co}}^N$  (which is compared with work by other authors using different methods: phase switch Monte Carlo, the non-equilibrium direct coexistence method, and the Einstein Molecule approach). We extrapolate  $p_{\text{co}}^{(N)}$  to the large  $N$  limit as  $p_{\text{co}}^{(N)} = p_{\text{co}}^\infty + a_1/N + a_2/N^2$  for  $256 \leq N \leq 2916$  ( $p_{\text{co}}^{N=4000}$  is compatible but not included in the fit because of dubious equilibration). The specific volume was extrapolated linearly in  $1/N$  ( $N \geq 256$  for the FCC and  $N \geq 500$  for the fluid).

In summary, we have introduced a tethered MC [26, 27] approach to HS crystallization. We go continuously from the fluid to the crystal by varying a reaction coordinate. Tethered MC provides a major simplification to umbrella sampling, which makes it possible to study multi-constrained free energies. At variance with previous methods, our simulations equilibrate (i.e. we find results independent of the starting particle configuration), not only for the formation of the space-filling crystal, but even for the more difficult case of mixed states with fluid-crystal interfaces. Our estimation of the coexistence pressure is, by far, the most accurate to date. That of the interfacial free energy is compatible with most (but not all) recent determinations. Should one wish to reach larger  $N$ , the tethered strategy would easily accommodate additional order parameters. The method can also be generalized to other simple liquids, or to investigate the glass transition.

## ACKNOWLEDGMENTS

We thank K. Binder, C. de Vega, L.G. MacDowell, B. Lucini and D. Yllanes for enlightening discussions. Simulations were carried out at BIFI. We acknowledge support from MICINN, Spain, through research contracts FIS2009-12648-C03, FIS2008-01323 and from UCM-Banco de Santander. B.S. was supported by FPU program.

## Appendix A: Extended simulation details

We provide some additional details for the interested reader. In particular, we give information necessary to reproduce our analysis and/or our simulations.

As shown in the Fig. 2, we take a segment of the straight line in the  $(\hat{Q}_6, \hat{C})$  plane that joins the fluid and the FCC minima of the effective potential. This segment is divided evenly in a grid of  $N_S$  points ( $N_S = 42$  for  $N \leq 1372$ , while  $N_S = 82$  for  $N \geq 2048$ ). All  $N_S$  points are simulated at the same pressure  $p$  (see Table I). We selected these  $p$  values by means of short, preliminary simulations.

At each of the  $N_S (\hat{Q}_6, \hat{C}, p)$  points, we run two independent simulations with different initial conditions, an ideal gas and a perfect FCC crystal. Each of the  $2 \times N_S$  runs had a length of  $10^6$  MC steps (1 MC step is composed of  $N$  particle displacements followed by one volume-change attempt). In addition, we show in Table I some  $N$ -dependent observables computed in the simulation, as well as the large- $N$  extrapolation. In order to ease comparison, we also tabulate the  $p_{\text{co}}^{(N)}$  values obtained by other groups (using different approaches).

## Appendix B: Geometrical transitions

As discussed in the main text, in a system with periodic boundary conditions, geometrical transitions arise when the line parameter  $S$  varies from the liquid to the solid. In fact, the system struggles to minimize the surface energy while respecting the global constraints for  $Q_6$  and  $C$ . Depending on the fraction of crystal phase, which is fixed by  $S$ , the minimizing geometry can be either a bubble, a cylinder or a slab of liquid in a crystal matrix (or vice versa). An example of each type of configuration is displayed in Fig. 4. As  $S$  varies, the minimizing geometry changes at definite  $S$  values. This phenomenon is named *geometric transition*, and has been previously studied in simpler models (for instance, first-order transitions in lattice magnetic systems, or fluid-gas phase-coexistence).

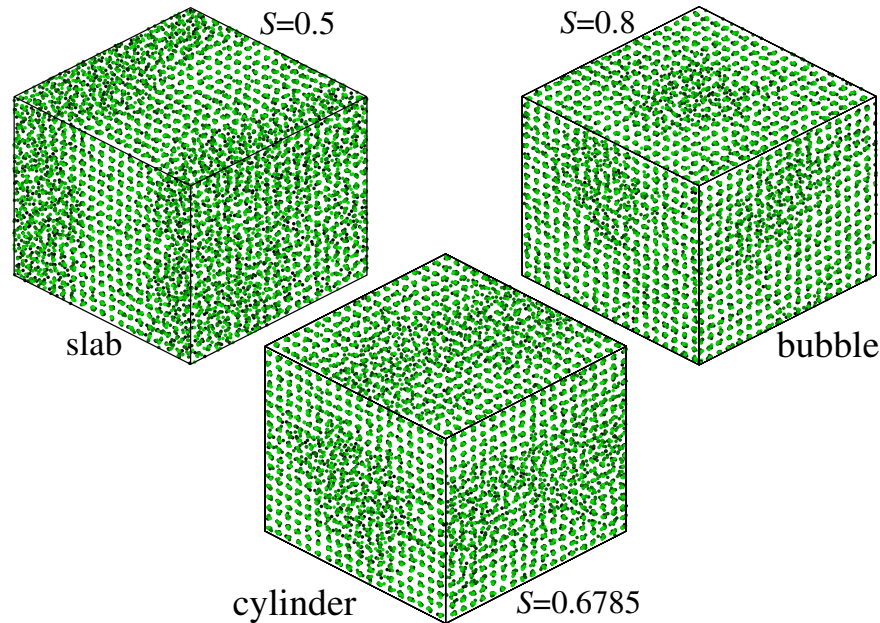


FIG. 4. Snapshots of mixed configurations for  $N = 2916$  particles found as the line parameter  $S$  varies. We present projections in the three Cartesian directions. To improve visibility, the radii are a fraction of the real ones, and the darkness is an increasing function of the distance to the projection plane.

- 
- [1] B. J. Alder and T. E. Wainwright, *J. Chem. Phys.* **27**, 1208 (1957); W. W. Wood and J. D. Jacobson, *ibid.* **27**, 1207 (1957).
- [2] P. N. Pusey and van Meegen, *Nature* **320**, 340 (1986).
- [3] P. N. Pusey, W. van Meegen, P. Bartlett, B. J. Ackerson, J. G. Rarity, and S. M. Underwood, *Phys. Rev. Lett.* **63**, 2753 (1989).
- [4] A. B. Manoharan, M. T. Elsesser, and D. J. Pine, *Science* **301**, 483 (2003); S. Glotzer and M. J. Solomon, *Nat. Mater.* **6**, 557 (2007).
- [5] E. Bianchi, J. Largo, P. Tartaglia, E. Zaccarelli, and F. Sciortino, *Phys. Rev. Lett.* **97**, 168301 (2006).
- [6] F. Sciortino, A. Giacometti, and G. Pastore, *Phys. Rev. Lett.* **103**, 237801 (2009).
- [7] M. P. Allen and D. J. Tildesley, *Computer Simulation of Liquids*, 2nd ed. (Oxford University Press, New York, 1989).
- [8] E. Zaccarelli, C. Valeriani, E. Sanz, W. C. K. Poon, M. E. Cates, and P. N. Pusey, *Phys. Rev. Lett.* **103**, 135704 (2009).
- [9] B. A. Berg and T. Neuhaus, *Phys. Rev. Lett.* **68**, 9 (1992).
- [10] F. Wang and D. P. Landau, *Phys. Rev. Lett.* **86**, 2050 (2001).
- [11] V. Martin-Mayor, *Phys. Rev. Lett.* **98**, 137207 (2007).
- [12] V. J. Anderson and H. N. W. Lekkerkerker, *Nature* **416**, 811 (2002).
- [13] C. Vega, E. Sanz, J. L. F. Abascal, and E. G. Noya, *J. Phys.: Condens. Matter* **20**, 153101 (2008).
- [14] N. B. Wilding and A. D. Bruce, *Phys. Rev. Lett.* **85**, 5138 (2000).
- [15] J. R. Errington, *J. Chem. Phys.* **120**, 3130 (2004).
- [16] W. G. Hoover and F. H. Ree, *J. Chem. Phys.* **49**, 3609 (1968).
- [17] D. Frenkel and A. K. C. Ladd, *J. Chem. Phys.* **81**, 3188 (1984).
- [18] J. M. Polson, E. Trizac, S. Pronk, and D. Frenkel, *J. Chem. Phys.* **112**, 5339 (2000).
- [19] C. Vega and E. G. Noya, *J. Chem. Phys.* **127**, 154113 (2007).
- [20] J. C. Ladd and L. V. Woodcock, *J. Chem. Phys.* **51**, 155 (1977).
- [21] E. G. Noya, C. Vega, and E. de Miguel, *J. Chem. Phys.* **128**, 154507 (2008).
- [22] T. Zykova-Timan, J. Horbach, and K. Binder, *J. Chem. Phys.* **133**, 014705 (2010).
- [23] R. L. Davidchack, *J. Chem. Phys.* **133**, 234701 (2010).
- [24] A. Cacciuto, S. Auer, and D. Frenkel, *J. Chem. Phys.* **119**, 7467 (2003).
- [25] Y. Mu, A. Houk, and X. Song, *J. Phys. Chem. B* **109**, 6500 (2005).
- [26] L. A. Fernandez, V. Martin-Mayor, and D. Yllanes, *Nucl. Phys. B* **807**, 424 (2009).
- [27] V. Martin-Mayor, B. Seoane, and D. Yllanes, *J. Stat. Phys.* **144**, 554 (2011).
- [28] G. M. Torrie and J. P. Valleau, *Chem. Phys. Lett.* **28**, 578 (1974); *J. Comp. Physics.* **23**, 187 (1977); C. Bartels, *Chem. Phys. Lett.* **331**, 446 (2000).
- [29] P. ten Wolde, M. J. Ruiz-Montero, and D. Frenkel, *Phys. Rev. Lett.* **75**, 2714 (1995).
- [30] M. Schrader, P. Virnau, and K. Binder, *Phys. Rev. E* **79**, 061104 (2009).
- [31] K. Binder, B. Block, S. K. Das, P. Virnau, and D. Winter, (2011), arXiv:1103.2241.

- [32] P. J. Steinhardt, D. R. Nelson, and M. Ronchetti, *Phys. Rev. B* **28**, 784 (1983).
- [33] J. S. van Duijneveldt and D. Frenkel, *J. Chem. Phys.* **96**, 4655 (1992).
- [34] S. Angioletti-Uberti, M. Ceriotti, P. D. Lee, and M. W. Finnis, *Phys. Rev. B* **81**, 125416 (2010).
- [35] M. Biskup, L. Chayes, and R. Kotecký, *Europhys. Lett.* **60**, 21 (2002).
- [36] K. Binder, *Physica A* **319**, 99 (2003).
- [37] L. G. MacDowell, V. Shen, and J. R. Errington, *J. Chem. Phys.* **125**, 034705 (2006).
- [38] P.-G. Bolhuis, D. Frenkel, S. C. Mau, and D. A. Huse, *Nature* **388**, 235 (1997).
- [39] Particles  $i$  and  $j$  are *neighbors* if  $r_{ij} < 1.5 \sigma$ . In the ideal FCC structure, for all particle-densities relevant to us, this choice includes only the nearest neighbors shell.
- [40] Eq. (7) behaves as an animal's tether: only if (say)  $|\hat{Q}_6 - Q_6(\mathbf{R})| \gg 1/\sqrt{N\alpha}$  is the penalty large. Note as well that Eqs. (7,8) generalize straightforwardly to the case of more than two quasi-constraints.
- [41] A magnitude  $A$  is *additive* if  $NA$  is extensive: gluing together systems 1,2 (with  $N^{(i)}$  particles and  $A = A^{(i)}$ ,  $i = 1, 2$ ), results in a total system with  $N = N^{(1)} + N^{(2)}$  particles and  $NA = N^{(1)}A^{(1)} + N^{(2)}A^{(2)}$  (plus subdominant corrections such as surface effects  $\sim N^{2/3}$ ).  $C$  is additive to a great accuracy for coexisting fluid and FCC phases, because the average number of neighbors  $N_b$  is very similar in both phases (5% difference, with negligible effects on additivity in our  $N$  range, as compared with surface effects).  $Q_6$  is additive only if one of the subsystems, say  $i = 1$ , is a liquid so that  $Q_6^{(1)} \sim 1/\sqrt{N^{(1)}}$  ( $Q_6$  is a pseudo-order parameter, i.e. a strictly positive quantity which is of order  $1/\sqrt{N}$  in a disordered phase). For studies of interfaces on larger systems, it would be advisable to choose exactly additive order parameters.
- [42] D. Ruelle, *Statistical Mechanics* (Benjamin, 1969).
- [43] Our runs for  $N \leq 2916$  are, at least,  $100\tau$  long ( $\tau$  is the integrated autocorrelation time [49], computed for  $Q_6$  and  $v$  [27]). For  $N = 2916$ , but only at  $S = 0.4$ , we find metastability with a helicoidal configuration (however, its contribution to final quantities is smaller than statistical errors). Metastabilities arise often for  $N = 4000$ , at intermediate  $S$  (yet, a careful selection of starting configurations yields a  $\nabla\Omega_N$  with smooth  $S$  dependency).
- [44] A. M. Ferrenberg and R. H. Swendsen, *Phys. Rev. Lett.* **61**, 2635 (1988).
- [45] C. Borgs and R. Kotecký, *Phys. Rev. Lett.* **68**, 1734 (1992).
- [46] The tethering approach should not induce artificial interfaces. In fact, mathematically, the interfacial free-energy is defined though the ratio of two partition functions with different boundary conditions. The tethered potential does not change the partition function [with any boundary conditions, see Eq. (5)].
- [47] K. Binder, *Phys. Rev. A* **25**, 1699 (1982).
- [48] A. Billoire, T. Neuhaus, and B. Berg, *Nucl. Phys. B* **413**, 795 (1994).
- [49] A. D. Sokal, in *Functional Integration: Basics and Applications (1996 Cargèse School)*, edited by C. DeWitt-Morette, P. Cartier, and A. Folacci (Plenum, N.Y., 1997).